Zigzag domain boundaries in magnetostrictive Fe-Ga alloys

Matthew N. Tianen [,1] Keat G. Ong,[2] and Yongmei M. Jin [1,*]

[1]*Department of Materials Science and Engineering, Michigan Technological University, Houghton, MI 49931, USA*
[2]*Phil and Penny Knight Campus for Accelerating Scientific Impact, University of Oregon, Eugene, Oregon 97403, USA*

A recent development in magnetic materials research on a non-Joulian magnetostriction phenomenon [H. D. Chopra and M. Wuttig, Nature **521**, 340 (2015)] highlights peculiar cellular magnetic domains with zigzag boundaries in Fe-Ga alloys. The cause of zigzag boundaries of cellular domains is attributed to hypothetical charge density waves beyond classical magnetic domain theory. In this paper, we report observations in Fe-Ga alloys of zigzag boundaries that form conventional stripe domains. The responses of stripe domains to external magnetic fields are observed, and the behaviors of zigzag boundaries are examined, which are further compared with those in cellular domains. It shows that both cellular and stripe domains and the constituent zigzag boundaries in magnetostrictive Fe-Ga alloys can be explained well by classical magnetic domain theory, without resorting to theory based on hypothetical charge density waves. In particular, our findings provide convincing evidence that zigzag boundaries in Fe-Ga alloys are conventional V lines commonly observed in cubic magnetic crystals like Fe-Si alloys. The intricate cellular domain structure is shown to correlate with the simple stripe domain structure in terms of zigzag V lines and flux-closure surface domains.

I. INTRODUCTION

Fe-Ga alloys, also known as Galfenol, exhibit high magnetostriction and good ductility. For example, single-crystalline Fe-Ga alloys were shown to exhibit in ⟨100⟩ crystallographic directions a high magnetostriction up to ∼400 ppm [1] and a yield strength of 515 MPa as well as 2% elongation [2]. This makes Galfenol more machinable than brittle magnetostrictive Terfenol-D [3], piezoelectric PZT [4], and magnetic shape memory Ni-Mn-Ga [5] and therefore suitable for a variety of actuator and sensor applications. Recently, Fe-Ga alloys have attracted even more interest for being a class of magnets exhibiting so-called non-Joulian magnetism (NJM), a discovery reported in *Nature* [6]. This class of magnets is claimed to exhibit desirable magnetization curves (hysteresis free, linearly reversible, and isotropic) due to unusually adaptive cellular magnetic domains [6,7]. One key feature of these cellular domains is their zigzag boundaries, the origin of which was attributed to hypothetical charge density waves [6,7]. The appealing discovery of NJM and especially interpretation of cellular magnetic domains using hypothetical charge density waves, however, needs further validation. Whether zigzag domain boundaries in Fe-Ga alloys are truly caused by charge density waves rather than being explained by classical magnetic domain theory is a crucial question to answer.

Zigzag domain boundaries in Fe-Ga alloys were reported in a single crystal of quenched 26.1 at.% Ga [6], where they were shown to form a periodic cellular domain pattern. The zigzagging feature was explained by the existence of hypothetical charge density waves, as illustrated in Fig. 1(a) [6].

Subsequently, similar cellular domains consisting of zigzag boundaries were observed in single-crystal specimens of slow-cooled 26.1 at.% Ga [7], quenched 17.1 at.% Ga [7], and quenched 18.07 at.% Ga [8], as well as polycrystalline as-cast 19 at.% Ga [8]. Contrary to the interpretation by hypothetical charge density waves [6,7] as shown in Fig. 1(a), zigzag domain boundaries of cellular domains were interpreted as conventional V lines in cubic magnetic materials, as shown in Fig. 1(b) [8]. The hypothetical charge-density-wave–based explanation [6,7] lacks justification and needs validation. Since zigzag V lines are well established from the viewpoint of classical domain theory [9,10], the V-line–based interpretation seems more natural and better grounded. However, zigzag boundaries in Fe-Ga alloys have been observed only in association with the peculiar cellular domain pattern, while V lines were commonly observed and studied in the conventional stripe domain pattern in Fe and Fe-Si [10]. Therefore, it is intriguing to consider whether or not zigzag boundaries would actually form a stripe domain pattern in Fe-Ga alloys; if they do, it would provide further evidence for the V-line–based explanation of the cellular domain pattern.

So far zigzag boundaries have been observed on the (001) surface in Fe-Ga alloys of relatively high Ga compositions (∼17 at.% and above), and as mentioned, they were shown to form a cellular domain pattern [6–8]. This paper reports observations of zigzag boundaries that form a simple parallel stripe domain pattern in Fe-Ga at a lower Ga composition of 8.5 at.%. The responses of stripe domains and especially zigzag boundaries to magnetic fields perpendicular to the (001) surface have been examined, which were further compared with the behaviors of zigzag boundaries in cellular domains. Our findings build a needed connection between stripe domains and cellular domains in Fe-Ga alloys and further confirm
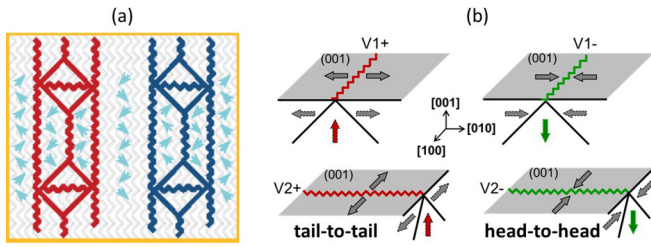
FIG. 1. Comparison between two contrasting models for zigzag domain boundaries in Fe-Ga alloys: (a) charge density wave model (reproduced with permission, Ref. [6]), and (b) V-line model [8]. In the V-line model, a zigzag boundary is the intersection of closure domains at the surface; red and green arrows correspond to [001] and [00$\bar{1}$] subsurface perpendicular domains, respectively.

the identity of zigzag boundaries as V lines, advancing our understanding of domain phenomena in Fe-Ga alloys which underlie their magnetoelastic behaviors.

II. EXPERIMENTAL DETAILS

Magnetic domains were observed on a specimen of as-grown Fe-8.5 at. % Ga single crystal prepared at Ames Lab. The specimen had a rectangular prism shape with {100} surfaces and was approximately $4 \times 2 \times 2 \, mm^3$ in size. Since Fe-Ga alloys are susceptible to surface damage [11], polishing Fe-Ga specimens must be done carefully with thorough rinsing of the specimen, polishing pad, and specimen holder between polishing steps. The specimen was mounted in epoxy, and a $4 \times 2 \, mm^2$ surface (referred to as the (001) surface hereafter) was polished using a Struers Labopol-1 autopolisher through the following steps: 800 grit SiC, 1 μm diamond paste on a Buehler Microcloth pad, 0.04 μm colloidal silica on an Allied High Tech White Label pad, and 0.04 μm colloidal silica on an Allied High Tech Imperial pad. The use of 0.04 μm silica on two different pads is unusual, but the White Label pad was found to be effective at removing larger scratches left by diamond polishing, while the Imperial pad was best at removing smaller scratches. On the polished surface, domain observation was performed by the Bitter method. Ferrotec EMG707 water-based ferrofluid was diluted 30:1 with distilled water. A drop was applied to the surface and covered with a glass coverslip, then observed under an optical microscope in Nomarski differential interference contrast mode. A perpendicular magnetic field along the [001] direction was applied using an electromagnetic coil placed below the sample.

III. RESULTS AND DISCUSSION

Figure 2(a) shows observed parallel stripe domains on the polished (001) surface of the as-grown Fe-8.5 at. % Ga single crystal. It is seen that stripe domains have zigzag boundaries of ~3 μm width; zigzagging details of boundaries are clearly visible from the zoomed-in image. Zigzag boundaries of stripe domains were commonly observed in cubic magnetic materials of Fe and Fe-Si and interpreted as V lines from the viewpoint of classical domain theory [10]. Therein, the magnetizations of stripe domains are oriented head-to-head
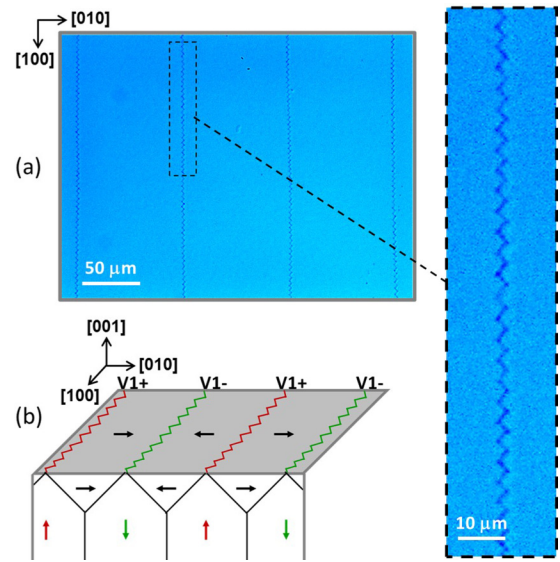

FIG. 2. Zigzag boundaries in as-grown Fe-8.5 at. % Ga single crystal. (a) Stripe domains observed on the (001) surface with a zoomed-in portion showing the zigzag boundary. (b) Interpretation of the stripe domain pattern with zigzag boundaries by the V-line model.

or tail-to-tail on the surface; boundaries between them are not regular domain walls but intersection lines where two subsurface 90° domain walls meet at the surface, and each of these intersection lines is a so-called V line, which caps a third domain of perpendicular magnetization beneath the surface, as illustrated in Fig. 2(b). The side view is a classical Landau pattern with closure domains at the surface to avoid the stray field that would otherwise be generated by internal perpendicular basic domains [10]. The V line on the surface was named after the V-shaped internal domain structure [12]. The zigzag feature of the V lines is caused by the zigzag folding of 90° domain walls in cubic magnetic materials with ⟨100⟩ easy directions [10]. The energetics of the zigzag folding of 90° domain walls was analyzed in Fe-Si by Chikazumi and Suzuki [9]. The V-line model of stripe domains with zigzag boundaries is well established. It is worth noting a recent experimental observation of the three-dimensional (3D) structure of zigzag V lines in Fe-12.8 at. % Si bulk crystals by Schäfer and Schinnerling [13] using the Libovický method to tomographically image a precipitation pattern that resembles a magnetic domain pattern.

In the V-line model [see Figs. 1(b) and 2(b)], zigzag boundaries on the (001) surface fall into two types depending on the magnetization orientation of the subsurface perpendicular domain, one pointing outward to [001] (red color) and the other pointing inward to [00$\bar{1}$] (green color), which correspond, respectively, to the tail-to-tail and head-to-head configuration on the surface. Zigzag V lines in stripe domains alternate in sequence between the two types. For the convenience of discussion, the V lines will be named V1+ and V1− (or V2+ and V2−), where V means V line, 1 (or 2) indicates the V line extending along the [100] direction (or [010] direction), and + indicates the subsurface perpendicular magnetization pointing out of the surface (the positive surface normal
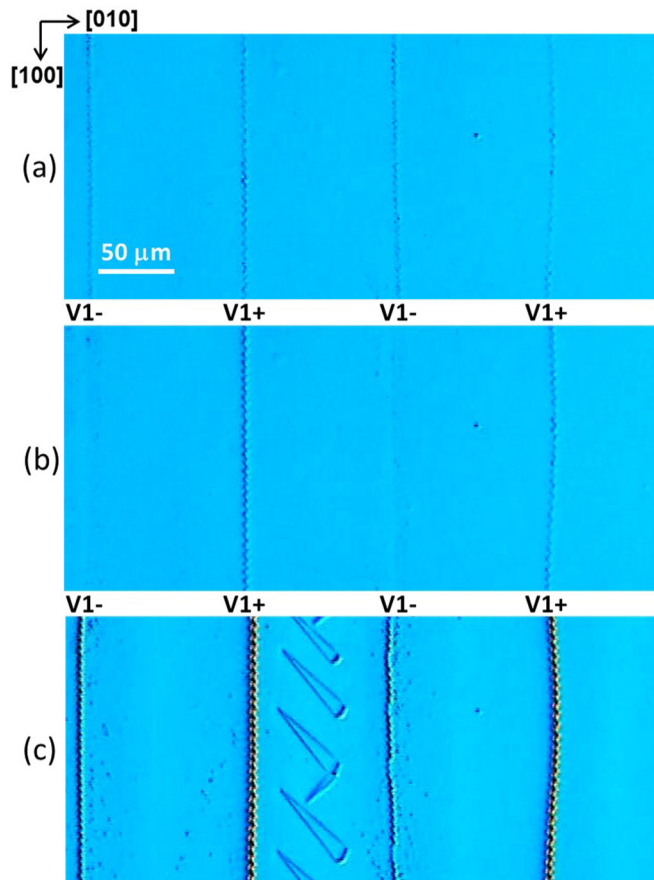
FIG. 3. Responses of zigzag boundaries of stripe domains to a [001] magnetic field in Fe-8.5 at. % Ga single crystal. (a) The same contrast of V1+ and V1− boundaries at $H^{ex} = 0$. (b) Enhancing of V1+ and fading of V1− boundaries at $H^{ex} = 8$ kA/m. (c) Enhancing of V1+ boundaries, reappearing of V1− boundaries, and emerging of spike domains at $H^{ex} = 52$ kA/m.

direction), while − indicates the opposite case, i.e., pointing into the surface (the negative surface normal direction). Because of the asymmetry of a V-line structure in terms of its subsurface perpendicular magnetization with respect to the surface, the two types of V lines, V1+ (V2+) and V1− (V2−) are expected to respond differently to a perpendicular magnetic field, depending on whether the subsurface magnetization and the magnetic field are parallel or antiparallel. Figure 3 presents an observation of the responses of stripe domains to a perpendicular magnetic field. Therein, the distinctive responses of V1+ and V1− conform to the asymmetry consideration.

Upon application of a small perpendicular magnetic field in the [001] direction, Fig. 3(b) shows that the contrast of zigzag boundaries enhances in one set of zigzag boundaries, while it fades away in the other set, in alternating sequence. As will be discussed later, the enhanced ones correspond to the subsurface magnetization parallel to the applied field, while the faded ones correspond to the subsurface magnetization antiparallel to the applied field. Specifically, under the [001] field, the enhanced V lines correspond to the V1+ type in red, while the faded V lines correspond to the V1− type in green, as shown in Fig. 2(b). Their distinct responses in Bitter

contrast may be explained by the agglomeration effect of ferrofluid particles under a perpendicular field (see chapter 2.2 in Ref. [10] for an in-depth discussion of the particle agglomeration effect). When a small perpendicular magnetic field is applied, the domain structure remains unchanged, while the Bitter particles form agglomerated chains with a higher susceptibility than isolated particles and thus become more sensitive to stray fields from domain boundaries below, which generally results in a stronger Bitter contrast of the domain boundaries with increasing field [10]. For this reason, an auxiliary field perpendicular to the surface was used to improve the Bitter image contrast. In the case of the applied field in the [001] direction, the particle chains align along the field direction perpendicular to the surface, with the north pole at the top end (far from the sample surface) and south pole at the bottom end (close to the sample surface). The south poles are attracted by the V1+ lines, where the magnetizations beneath are parallel to the [001] direction, while they are repelled by the V1− lines, where the magnetization beneath are antiparallel to the [001] direction, resulting in the fading contrast of V1− lines contrary to the enhancing contrast of V1+ lines. Interestingly, when the field magnitude is further increased, the faded set of V1− zigzag boundaries reappears, as shown in Fig. 3(c). Moreover, the contrast of the reappearing V1− zigzag boundaries is enhanced compared with that under zero field in Fig. 3(a). This is likely due to a field-induced change in the local magnetization distribution of the boundaries and thus the resultant stray field that alters the distribution of ferrofluid particles.

It is also seen in Fig. 3(c) that new domains of spiked shape emerge within stripe domains when the [001] magnetic field is increased to $H^{ex} = 52$ kA/m. These field-generated domains are like Néel spikes. Néel spikes were theoretically predicted for cubic magnetic crystals [14] and experimentally observed on the surface [15] and inside the volume (by Libovický tomography) [13] of Fe-Si, where they were formed in the vicinity of voids and nonmagnetic inclusions to accommodate the magnetic charges (i.e., to become charge free) at the surfaces or interfaces. The spike domains shown in Fig. 3(c) are also formed to accommodate magnetic charges, but these are not due to static crystal defects but from field-induced subsurface perpendicular domains, as illustrated in Fig. 4.
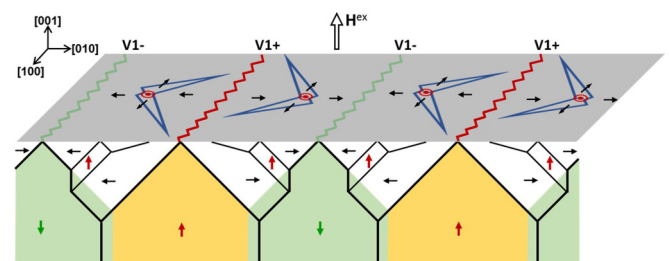

FIG. 4. Schematic illustration of spike domains on the (001) surface because of the formation of [001] domains within the V-shaped surface closure domains ([010] or [0$\bar{1}$0]) under a perpendicular [001] magnetic field. These [001] domains facilitate the [001] field-driven growth of basic perpendicular [001] domains (orange color under zero field) and shrinkage of basic perpendicular [00$\bar{1}$] domains (green color under zero field).
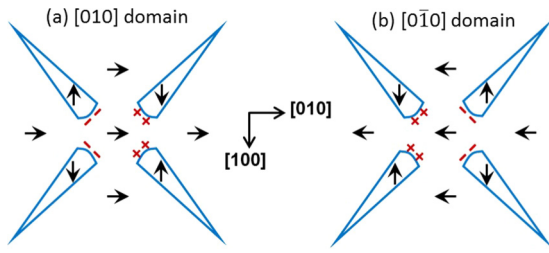
FIG. 5. Schematic illustration of spikes on the (001) surface within (a) [010] parent domain and (b) [0$\bar{1}$0] parent domain. A spike alone would create magnetic charges at its base if the underneath perpendicular domain were not present.

Therefore, while defect-induced Néel spikes are present at zero magnetic field, field-induced Néel spikes are not present at zero or small magnetic field, as shown in Figs. 3(a) and 3(b). These spikes are therefore external-field dependent and appear only when perpendicular domains ([001] or [00$\bar{1}$] depending on field direction) are formed within the V-shaped surface closure domains ([100], [$\bar{1}$00], [010], or [0$\bar{1}$0]).

Consider application of a [001] magnetic field (out of the surface) to the stripe domain structure shown in Fig. 2(b). To reduce the Zeeman energy, [001] domains form within the V-shaped surface closure domains, the [001] basic domains grow, and the [00$\bar{1}$] basic domains shrink, as illustrated in Fig. 4. These field-generated [001] domains in the V-shaped surface closure domains create positive magnetic charges at the surface. To accommodate these magnetic charges, spike domains with an in-plane magnetization form on the surface to cap these [001] domains. A spike with [100] (or [$\bar{1}$00]) magnetization forms a 90° head-to-tail magnetization configuration on the (001) surface, pointing to one of the four ⟨110⟩ directions, as exemplified for the [010] parent domain in Fig. 5(a) and for the [0$\bar{1}$0] parent domain in Fig. 5(b).

A spike alone creates magnetic charges at its base (could be positive or negative as illustrated in Fig. 5), which are accommodated when joined with a defect or an underneath perpendicular domain at the base. Among these spike branches, only the spikes that are shown to carry negative charges at the base can accommodate the [001] perpendicular domain (with the magnetization upward in Fig. 4, thus forming positive charges on the surface) through formation of a subsurface head-to-tail 90° wall in the vicinity of the spike base. They are the two branches pointing left in the [010] parent domain shown in Fig. 5(a) and the two pointing right in the [0$\bar{1}$0] parent domain shown in Fig. 5(b). In other words, two spike branches (among four) are selected for each parent domain, and they point against the magnetization direction of the parent domain. This leads to spikes in the stripe domains that alternate their pointing directions from stripe to stripe.

Now consider reversing the direction of the magnetic field to [00$\bar{1}$] (into the surface), thus creating [00$\bar{1}$] perpendicular domains in the V-shaped surface closure domains. Following the same charge accommodation mechanism, the pointing direction of the spikes on the surface must be switched, i.e., the other two spike branches are selected for each parent domain in Fig. 5. That is, the spikes point right in the [010] parent domain, while they point left in the [0$\bar{1}$0] parent domain. Again, two spike branches (among four) are selected in each

parent domain, and the spikes in the stripe domains alternate their pointing directions from stripe to stripe. The difference from the case of the [001] subsurface perpendicular domain is that now the two spikes in each parent domain point along (instead of against) the magnetization direction of the parent domain. The relations among the three directions, namely, the spike pointing direction, the magnetization direction of the surface parent domain, and the magnetization direction of the subsurface perpendicular domain formed inside the surface closure domain, can be summarized into a simple spike selection rule: the spikes point against the magnetization direction of the surface parent domain when the subsurface perpendicular magnetization points out of the surface under [001] field, while the spikes point along the magnetization direction of the surface parent domain when the subsurface perpendicular magnetization points into the surface under [0$\bar{1}$0] field. This simple rule is very useful in analyzing Bitter patterns. In the Bitter method, the spike-pointing direction is directly observed, the magnetization direction of the sub-surface perpendicular domain is known to be parallel to the applied field to reduce the Zeeman energy, and the spike selection rule allows us to conveniently determine the magnetization directions of both surface parent domains and spike domains, which cannot be determined by the Bitter method. Therefore, the spike selection rule is a concise summary of the domain structure features, in agreement with the general rule of magnetic domains, and is a useful tool for Bitter pattern analysis.

Consider Fig. 3(c), where spikes present in one stripe domain under a [001] magnetic field of $H^{ex} = 52$ kA/m. As expected, spikes of only two branches (pointing left) are present. Based on the spike selection rule (spikes pointing against the parent magnetization for [001] subsurface perpendicular magnetization), the parent stripe domain is a [010] type. As a result, the zigzag boundary on its left is a tail-to-tail V1+, and that on its right is a head-to-head V1− (see Fig. 2). When the magnetic field is increased, more spikes emerge in stripe domains, as exemplified in Fig. 6(a).

Figure 6(a) shows stripe domains filled with spikes under a [001] magnetic field of $H^{ex} = 70$ kA/m. Conforming to the spike selection rule, spikes alternate their pointing directions from stripe to stripe. It is also observed in Fig. 6(a) that the two types of zigzag boundaries remain distinct, the contrast of V1+ being sharper than V1−. For clarity, the corresponding schematics in Fig. 6(a′) show two spike branches pointing left in the [010] stripe domain and two spike branches pointing right in the [0$\bar{1}$0] stripe domain (all against their parent magnetizations), the in-plane magnetization vectors on the surface and the perpendicular magnetization vectors of the [001] subsurface domains beneath the spike bases, and zigzag boundaries with higher contrast in bright color (red V1+ in this case) and those with less contrast in dimmed color (green V1−). To demonstrate the effects of the external magnetic field direction on the domain behaviors, the field is reversed to [00$\bar{1}$], and the changes in the magnetic domains are seen in Fig. 6(b). The spike pointing direction is now reversed in individual stripes, and the contrast of the V1+ and V1− zigzag boundaries is also reversed, complying with the spike selection rule. In comparison with Fig. 6(a′), the characteristic domain features under the reversed magnetic field are also
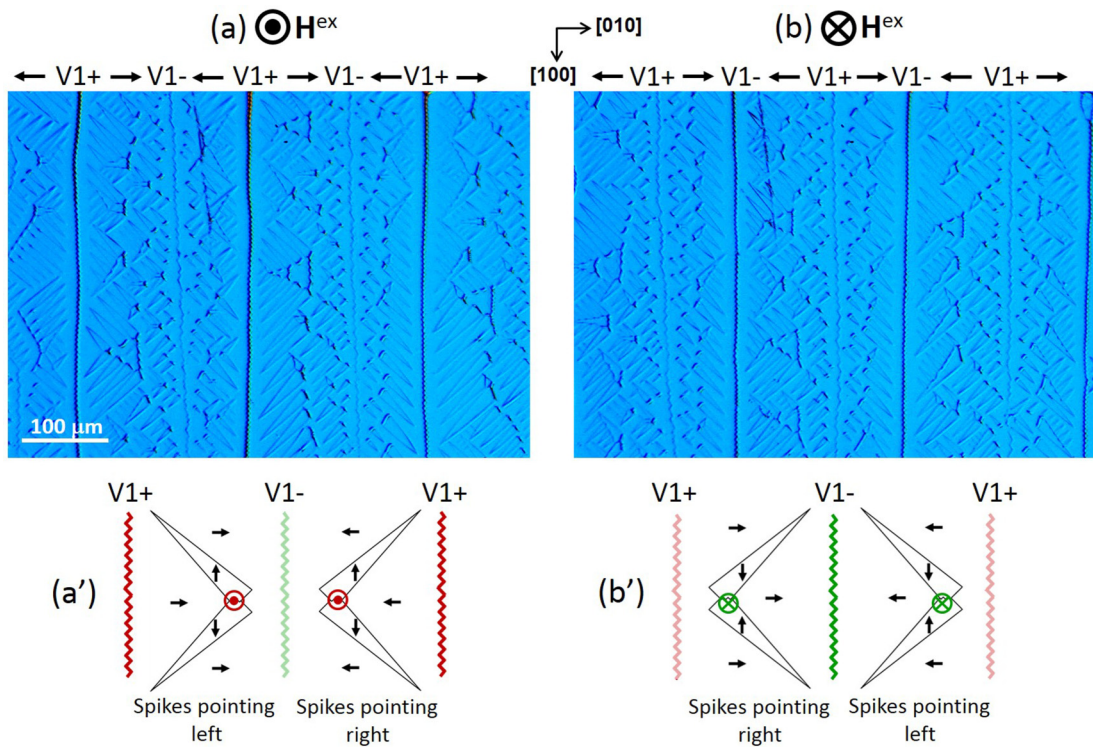
FIG. 6. Responses of zigzag domain boundaries and formations of spikes in Fe-8.5 at. % Ga single crystal under a magnetic field $H^{ex} = 70$ kA/m along (a) [001] (out of the surface) and (b) [00$\bar{1}$] (into the surface), respectively. (a′) and (b′) Schematics of two branches of pointing-left/pointing-right spikes, subsurface perpendicular magnetizations (red and green arrows) beneath the spike bases, and distinct contrasts (enhancing and fading) of zigzag V1+ and V1− boundaries in (a) and (b).

schematically illustrated in Fig. 6(b′). It is worth noting that, while a joined spike pair is exemplified within each stripe in Figs. 6(a′) and 6(b′), spikes in other configurations are also seen in Figs. 6(a) and 6(b), including separated single spikes and adjoined clusters with multiple spikes. Among them, two types of the spike clusters are of particular interest and are singled out in Fig. 7.

The two spike clusters shown in Fig. 7 are of particular interest because they show not only an impressive shape but also, more importantly, newly formed zigzag boundaries. The zigzag boundaries are seen to connect two spikes and have a length of a few zigzag periods, as highlighted by white dashed line loops in Figs. 7(a) and 7(b). Inspecting the two spike clusters closely, the first one in Fig. 7(a) features a closed body with a single zigzag boundary, while the second one in Fig. 7(b) features an open body with double zigzag boundaries. Given the external magnetic field in the [001] direction and the spikes pointing left in Figs. 7(a) and 7(b), the spike selection rule readily infers the magnetization distributions for these two domain structures, as shown in the corresponding schematics in Figs. 7(a′) and 7(b′). The closed body of the spike cluster is enclosed by one zigzag boundary and two stair-shaped boundaries, as shown in Fig. 7(a). Since this zigzag boundary exhibits strong contrast in Fig. 7(a), it is of tail-to-tail V1+ type. Each of the stair-shaped boundaries consists of regular charge-free 180° walls (horizontal segments) and 90° walls (inclined segments). It is worth mentioning that a similar domain structure to that seen in Fig. 7(a) was
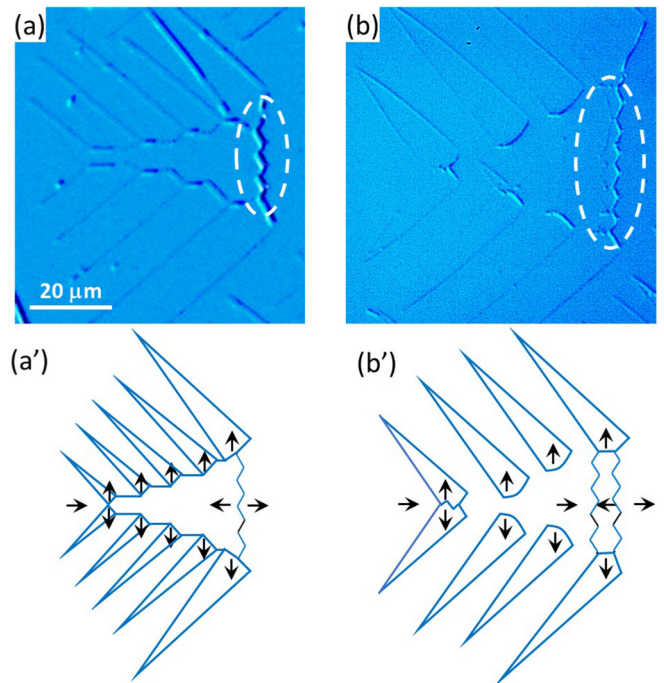

FIG. 7. Spike clusters formed under a magnetic field of 70 kA/m along [001]. They exhibit newly formed (a) single zigzag boundary and (b) double zigzag boundaries, which are highlighted with white dashed line loops. (a′) and (b′) Schematics of the magnetic domain structures corresponding to (a) and (b).

observed in Fe-Si and is called the fir tree pattern therein [10]. On the other hand, the spike cluster with open body in Fig. 7(b) is composed of separated spikes and a pair of zigzag boundaries. As seen in Fig. 7(b), between the two zigzag boundaries, the one on the right shows stronger contrast than the one on the left. Therefore, the right zigzag boundary is of tail-to-tail V1+ type, while the left one is of head-to-head V1− type. Beyond the well-known zigzag V lines of long length that form a simple stripe domain pattern, Fig. 7 demonstrates the field-induced zigzag V lines of short length, being part of the complex spike domain patterns.

It is also observed that the parallel stripes (i.e., the surface closure domains) become wider or narrower in an alternating sequence when the magnetic field increases. This is because the magnetic coil beneath the sample does not produce a perfectly perpendicular magnetic field, and the sample experiences a slight in-plane magnetic field component depending on the positioning of the sample, and the in-plane component increases as the field increases. The observed changes in the widths of the surface closure domains would be absent if a high-quality magnetic coil is used to apply a perfectly perpendicular magnetic field on the sample.

So far, the foregoing discussions and Figs. 2–7 have addressed the stripe domains parallel to the [100] direction and their zigzag boundaries of V1+ and V1− types. Imposing a 90° rotation to them results in stripe domains parallel to the [010] direction and their zigzag boundaries of V2+ and V2− types. Under perpendicular magnetic fields, the behaviors of V2+ and V2− zigzag boundaries are the same as V1+ and V1−, respectively, and the spike selection rule applies by replacing the pointing left and right with the pointing up and down, respectively. Due to the cubic symmetry of Fe-Ga alloys, stripe domains parallel to [100] and [010] are energetically equivalent, and both are observed on the $4 \times 2\,\mathrm{mm}^2$ (001) surface at different locations. It is observed in Figs. 2, 3, and 6 that the typical width of stripe domains is on the order of $\sim$100 μm, the size of perpendicular field-generated spike domains varies on the order of tens of micrometers, and the zigzagging width of the V lines is a few micrometers.

It is worth mentioning that the spike selection rule used above in analyzing the magnetic domains in Fe-Ga is a domain analysis tool based on magnetic energy consideration (to form charge-free surface and domain walls and reduce Zeeman energy and stray field energy). As a matter of fact, the spike selection rule is supported by the recent finding of the moth domain structure via a Libovický tomography study of Fe-12.8 at. % Si bulk crystal [13]. The moth domains were observed on a slightly misoriented (001) surface, whose structures are illustrated in Fig. 8 [13]. Due to the surface misorientation, the in-plane easy directions are not parallel to the surface, thus creating magnetic charges on the surface. In Fig. 8, the in-plane magnetization tips up (forming positive surface charges) in the left stripe, while it tips down (forming negative surface charges) in the right stripe. The resultant surface charges generate heterogeneous internal magnetic field beneath the surface, pointing down in the left stripe and pointing up in the right stripe. This internal magnetic field accounts for the subsurface perpendicular domains with downward magnetization in the left stripe and upward magnetization in the right stripe. In the left stripe, since the perpendicular
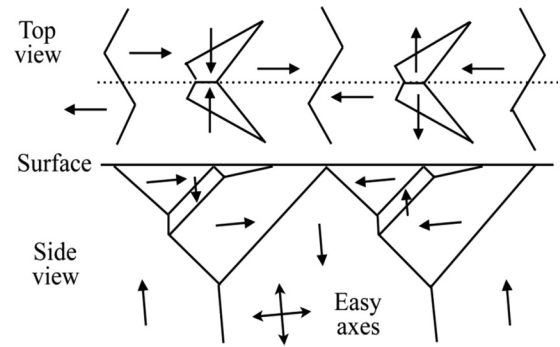

FIG. 8. Schematics of moth domain structure on a slightly misoriented (001) surface of Fe-12.8 at. % Si bulk crystal (reprinted figure with permission from Ref. [13]).

magnetization points into the surface, the spike selection rule dictates that the spikes point along the parent magnetization to the right; on the other hand, in the right stripe, since the perpendicular magnetization points out of the surface, the spike selection rule dictates that the spikes point against the parent magnetization to the right. In both stripes, these predictions agree with the experimental observations in Fe-Si alloys [13]. The spike selection rule can be also useful in analyzing Kerr patterns of moth domains: knowing the pointing direction of the moth wings and the magnetization direction of the surface parent domain, the direction of the subsurface perpendicular magnetization (thus, the internal demagnetization field) can be derived, which allows a determination of the tilting direction of the surface misorientation. Comparing the spike domain structure in Fig. 4 with the moth domain structure in Fig. 8, a main difference is that, when crossing from one stripe to the next, spikes switch pointing direction in the former while keep the same pointing direction in the latter because, in the former case, the subsurface perpendicular domains in the neighboring stripes have the same magnetization direction along the external field, while in the latter case, the subsurface perpendicular domains in the neighboring stripes have opposite magnetization directions along their respective internal perpendicular stray field directions that alternate between the stripes. Another main difference is that the basic domains widen or shrink in the case of applied perpendicular field in Fig. 4, while the basic domains remain intact in the case of surface misorientation in Fig. 8 because, in the latter case, the stray field caused by the surface misorientation extends only a small depth (approximately the size of the surface domains) beneath the surface, and there is no external field to drive the internal perpendicular basic domains to grow or shrink. The spike selection rule consistently explains both the field-induced spike domains in Fe-Ga and the surface misorientation-induced moth domains in Fe-Si simply based on the field (external or internal)-selected perpendicular domains in the V-shaped surface closure domains. Based on the analogies between the spike domain pattern in Fe-Ga and the moth domain pattern in Fe-Si, they are essentially the same type of surface domain structure, where the former is induced by a perpendicular external magnetic field, while the latter is caused by the internal stray field due to surface misorientation. It is also noted that the perpendicular field-induced spike
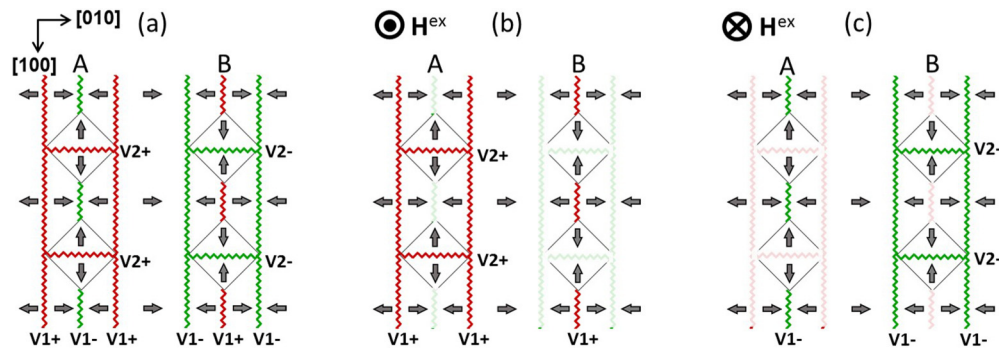
FIG. 9. (a) V-line model of cellular domains in Fe-Ga alloys [8]. Predicted responses of V lines under magnetic field along (b) [001] (out of the surface) and (c) [00$\bar{1}$] (into the surface).

domains in Figs. 3 and 6 are narrower with pointy shape, while the surface misorientation-induced moth domains are wider with greater wedge angle [10,13], and the mechanism for such a shape difference requires a further quantitative study of the energetics of Fe-Ga and Fe-Si, including the magneto-static, elastic, exchange interactions, and magnetocrystalline anisotropy.

Having interpreted zigzag boundaries in stripe domains in Fe-8.5 at. % Ga as conventional V lines, we next consider the zigzag boundaries observed in Fe-Ga alloys of higher com-positions which exhibit cellular domains. Interpreting zigzag boundaries in cellular domains of Fe-Ga alloys has aroused a controversy: a model based on hypothetical charge den-sity waves [6,7] versus a conventional model based on the well-established V lines [8]. In the following, the behavior of zigzag boundaries in cellular domains is compared with that in stripe domains, based on which the two models are discussed on their respective merits.

Cellular domains observed in Fe-Ga alloys consist of reg-ularly spaced chains of cells that run parallel to the [100] (or [010]) direction on the (001) surface [6–8]. Each cell consists of a rectangular-shaped outer zigzag borderline and a zigzag centerline that is connected to the outer rectangle corners by straight lines (these lines are hardly visible under zero field but can become visible under perpendicular mag-netic fields, i.e., auxiliary fields, at higher magnification, as demonstrated in Ref. [8]). According to the V-line model of cellular domains [8], the zigzag borderline and centerline are V lines, and the straight lines are charged 90° domain walls, as illustrated in Fig. 9(a). There are four types of V lines in cellular domains, V1+ and V2+ capping [001] subsurface perpendicular domains, and V1− and V2− capping [00$\bar{1}$] subsurface perpendicular domains, as shown in Fig. 1(b). Two types of cells are shown to alternate between the chains, which will be called cell A and B (chain A and B, correspondingly) for brevity. Cell A has a red zigzag borderline (V1+ and V2+) with a green zigzag centerline (V1−), while cell B has a green zigzag borderline (V1− and V2−) with a red zigzag centerline (V1+). A 3D view of the V-line model of cellular domains is presented in Fig. 10(a) in direct comparison with that of stripe domains in Fig. 2(b). The side view of the cellular domains in Fig. 10(a) shows a Landau pattern with closure domains formed to accommodate internal perpendic-ular basic domains, like the case of stripe domains. To aid in visualization of individual compartments of the cellular

domain structure, a 3D exploded view [16] is presented in Fig. 10(b), where the wedge-shaped surface domains (with magnetizations along ±[100] and ±[010] directions) have been removed from the internal perpendicular basic domains (with magnetizations along ±[001] directions) and shown separately on top. Due to the magnetostriction, each domain elongates in the magnetization direction, while it contracts in its perpendicular directions, and the six magnetic domains result in three strain states shown in three different colors. Fitting the surface domains into the space adjoining the in-ternal perpendicular basic domains causes elastic deformation
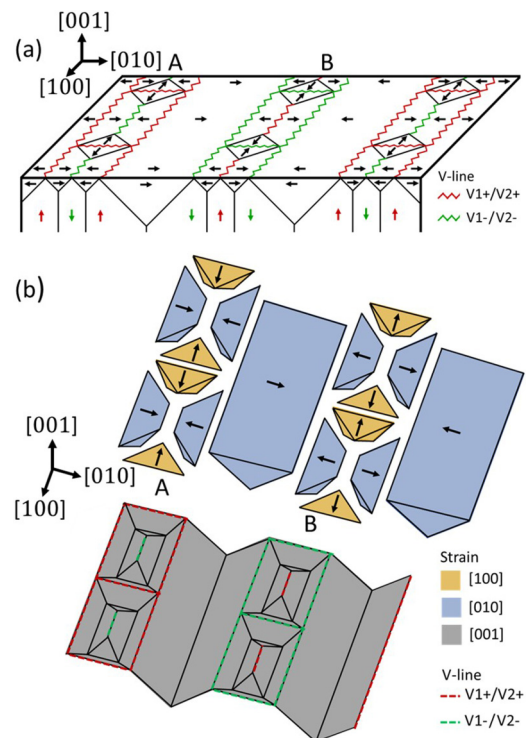

FIG. 10. Three-dimensional (3D) views of the V-line model of cellular domains in Fe-Ga alloys (reproduced with permission from Ref. [16]). (a) Top view with zigzag V-lines and side view with clo-sure domains. (b) Wedge-shaped surface domains shown separately must elastically deform to fit into the space above and between the internal perpendicular basic domains. The magnetization is shown by arrows and the strain state by filled colors.
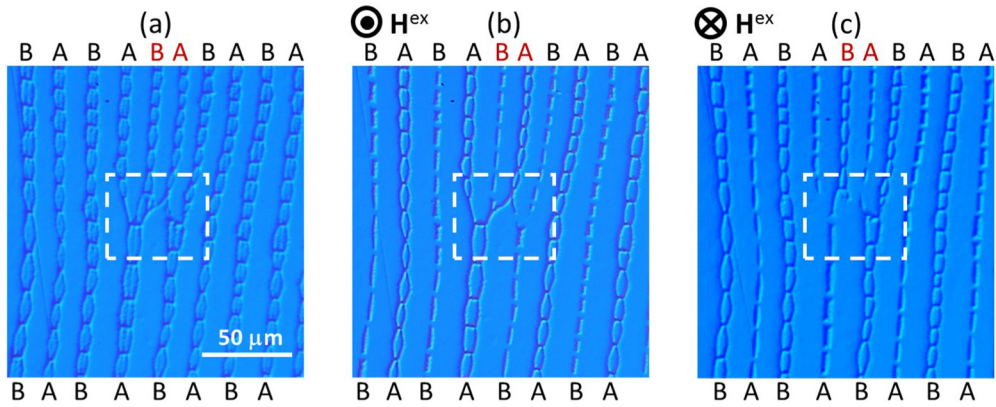
FIG. 11. Responses of cellular domains on the (001) surface in quenched Fe-18.07 at. % Ga single crystal to perpendicular magnetic fields: (a) 0 G, (b) 8 kA/m along [001] (out of the surface), and (c) 8 kA/m along [00$\bar{1}$] (into the surface).

and generates elastic energy. Because the misfit strains of the $\pm[100]$ and $\pm[010]$ surface domains compensate each other with respect to the strain state of the $\pm[001]$ perpendicular basic domains, a mixture of the two surface domain strain states lowers the overall misfit with the internal perpendicular basic domains. The cellular domain structure forms to lower the elastic energy by periodically alternating between $\pm[100]$ and $\pm[010]$ surface domains, but at the cost of charged 90° domain boundaries between them. As shown in Fig. 10(b), the charged 90° domain boundaries are misfit strain-free (110) and (1$\bar{1}$0) walls of triangular shape. The energy cost incurred by these charged 90° domain walls is small because they extend only a small depth, a fraction of the cell size, beneath the surface; the cell size in the transverse direction of the chains is usually below 10 μm in Fe-Ga alloys [6–8]. In essence, the cellular domain structure reduces the elastic energy as compared with the stripe domain structure by decreasing the surface domain size ($\sim$10 μm vs $\sim$100 μm as seen in Figs. 3 and 11), thus reducing the volume of elastically unfavorable closure domains, and by mixing the two compensating strain states of the surface domains, thus reducing their overall strain misfit with the internal perpendicular domains, while increasing the domain wall energy for creating additional domain walls. Therefore, the cellular domain structure is preferred over the stripe domain structure when the elastic energy dominates (e.g., stronger magnetostriction). The magnetostriction in Fe-Ga alloys exhibits a strong composition dependence, and indeed, the simple stripe domain pattern is observed at a lower Ga concentration (8.5 at. % Ga), as in this paper, where the magnetostriction is small ($\lambda_{100} \sim 75$ ppm), while the periodic cellular domains are observed at higher Ga concentrations (17.01–26.1 at. % Ga), where the magnetostriction is large ($\lambda_{100} \gtrsim 200$ ppm) [6–8]. Moreover, a range of transitioning domain patterns between these two patterns, the so-called cellular domain variations, have been recently observed at an intermediate Ga concentration of 15 at. % Ga [16]. A transition from the simple stripe domain pattern to the finer cellular domain pattern observed on the surfaces is accompanied by decreasing sizes of internal perpendicular basic domains beneath the surfaces. Therefore, domain branching of internal perpendicular basic domains leads to cellular domains on the surfaces, and the cellular domain pattern is a special branching pattern of the simple stripe domain structure.

Despite the complex 3D geometry of cellular domains, their responses to a perpendicular magnetic field can be readily predicted on the sample surface, according to the zigzag V line behavior learned from simple stripe domains. Under [001] magnetic field, the V1− and V2− are expected to fade, and as a result, cell A will show only its borderline without the centerline (i.e., border only), while cell B will show only its centerline without the borderline (i.e., center only), as illustrated in Fig. 9(b). Correspondingly, chain A will become a chain of empty cells (i.e., border-only cells), while chain B will become a chain of disconnected centerlines (i.e., center-only cells resembling a dashed line). When the magnetic field is reversed to the [00$\bar{1}$] direction, as shown in Fig. 9(c), the domain pattern is expected to be reversed: center only for cell A (dashed line for chain A) and border only for cell B (empty cells for chain B). This prediction can be tested experimentally in Fe-Ga single crystals of higher compositions where cellular domains are present.

The prediction illustrated in Fig. 9 is experimentally confirmed by magnetic domain observations in a quenched Fe-18.07 at. % Ga single crystal [8]. Figure 11(a) shows the cellular domain pattern of many cells that form long parallel chains on the (001) surface of the quenched Fe-18.07 at. % Ga single crystal under zero magnetic field. The responses of cellular chains to a [001] magnetic field shown in Fig. 11(b) and to the reversed [00$\bar{1}$] field shown in Fig. 11(c) fully comply with the prediction from the V-line model of cellular domains. Specifically, the chains are observed to alternate between empty cells and dashed lines under a perpendicular field, and the pattern switches when the field is reversed. Each chain is identified as A or B type, based on its response to the perpendicular magnetic field. For example, under [001] field, the border-only (empty cell) chains are of A type, while the center-only (dashed line) chains are of B type. In the periodic cellular domain structure in Fig. 11, it is interesting to notice a defect, which is highlighted by the white dashed rectangle. It is caused by the introduction of an extra pair of half-chains (marked as B and A in red) midway through the cellular domains. This defect is an analogy of the edge dislocation in a crystal. In the V-line model, chains A and B must alternate as shown in Fig. 9(a), so extra chains must be introduced in pairs. As seen in Fig. 11, the "dislocation core" features some irregular domain structure with the two extra

half-chains merging with their neighboring complete chains to transition from the upper four chains (ABAB) to the lower two chains (AB). Such a "dislocation" would very likely serve as a nucleation site for domain pattern changes, like a switching between vertical chains (parallel to [100]) to horizontal chains (parallel to [010]) observed under in-plane magnetic fields [6], which deserves further investigation.

The V-line model enables us to correlate intricate cellular domains with simple stripe domains in Fe-Ga alloys and explain the behaviors of zigzag boundaries that are common to them. A natural question is then whether the same is true for Fe-Si alloys, in which stripe domains have been extensively reported, while cellular domains are much less known. Indeed, we surprisingly came across Stephan's comprehensive study of cellular domains (not so called though) on (001) surfaces of Fe-Si [17,18]. Stephan not only observed the cellular domain phenomenon but also derived the magnetic structure in 3D. The Stephan model is the same as the above-discussed V-line model of cellular domains near the surface in Fig. 10 and even goes further to include the branching feature of perpendicular basic domains deep under the surface. The important findings by Stephan on cellular domains in Fe-Si have not received attention until very recently [8]. Furthermore, a side view of cellular domains in Fe-12.8 at. % Si (named chain domains therein), which has just become available via the Libovický's tomography study by Schäfer and Schinnerling [13], matches the 3D cellular domain structure predicted by Stephan, including the branching feature of perpendicular basic domains. This provides pivotal evidence for the identity of zigzag boundaries in cellular domains in Fe-Si. As a matter of fact, the branching pattern of cellular domains resembles the branching pattern of chainlike domains observed in Fe-Si alloys on (110) surfaces under in-plane magnetic field along the [$\bar{1}$10] direction, as shown in figure 5.22 in Ref. [10]. Therein, the increased strain misfit between surface domains and internal basic domains with increased external field accounts for the branching of internal basic domains and miniaturizing of surface domains. These findings in Fe-Si [10,13,17,18] confirm the generic aspects of cellular domains (i.e., stress accommodating surface domains) in ironlike cubic magnetic crystals and corroborate the V-line interpretation of zigzag boundaries in Fe-Ga.

The model based on hypothetical charge density waves [6,7], on the other hand, cannot explain the observed zigzag boundary behaviors under perpendicular magnetic fields. In this model shown in Fig. 1(a), borderline and centerline zigzag boundaries of a cell are equivalent with respect to a perpendicular magnetic field, which contradicts their distinctive responses to a perpendicular magnetic field observed in experiments (see Figs. 9 and 11). Moreover, in the charge-density-wave–based model, the conventional 180° domain walls parallel to the ⟨100⟩ easy axes are forbidden, which directly contradicts the very existence of straight 180° domain walls without zigzags, as widely observed in Fe-Ga alloys of compositions 15.8–19 at. % Ga [11,19–21]. Furthermore, the charge-density-wave–based model considers cellular domains as bulk domains that extend into the crystal volume, while cellular domains in the V-line–based model are merely surface domains that exist only on the surface. The tomography

study by Schäfer and Schinnerling [13] provides unambiguous experimental evidence of cellular domains being surface domains and zigzag lines being V lines in Fe-Si. Finally, the charge-density-wave–based model cannot explain the above-discussed conventional stripe domains and the formation of spikes in the stripes in Fe-Ga alloys.

IV. CONCLUSIONS

In this paper, zigzag domain boundaries in Fe-Ga alloys were investigated using magnetic domain observation experiments via the Bitter method. Zigzag boundaries were shown to form conventional stripe domains on the (001) surface of an as-grown Fe-8.5 at. % Ga single crystal. The responses of stripe domains to perpendicular magnetic fields were examined, revealing the behaviors of zigzag boundaries and the formation of spike domains in the stripes. Different types of zigzag boundaries of the stripes were identified based on their distinctive behaviors, nucleation of zigzag boundaries within the stripes were unveiled, and a simple spike selection rule was established for perpendicular field-induced spikes. Based on the analysis of the observed stripe domain phenomena and their relation to well-studied stripe domains in similar cubic magnetic systems of Fe-Si, zigzag boundaries in Fe-8.5 at. % Ga were confirmed to be the well-known V lines from classical domain theory. Subsequently, the behaviors of zigzag boundaries in stripe domains are compared with those in cellular domains previously observed in Fe-Ga alloys of higher Ga compositions. A quenched Fe-18.07 at. % Ga single crystal was used to demonstrate the same zigzag boundary behaviors, providing clear evidence that zigzag boundaries in cellular domains are also V lines. An interesting dislocationlike defect in the highly periodic cellular domain pattern was discussed considering the V-line interpretation of the cellular domain structure. The results by Stephan [17,18] and the recent magnetic domain tomography study by Schäfer and Schinnerling [13] on cellular domains in Fe-Si further confirm the V-line model of zigzag boundaries of cellular domains in Fe-Ga. Our findings disapprove the charge-density-wave–based model of cellular domains in magnetostrictive Fe-Ga alloys, where the origin of zigzag boundaries is attributed to hypothetical charge density waves beyond classical magnetic domain theory, thus resolving the controversy between the V-line–based model and the charge-density-wave–based model of zigzag boundaries and advancing our understanding of magnetic domains in Fe-Ga alloys. Finally, it is worth noting that the models of spike domains and cellular domains presented in this paper are based on intuitive arguments of the energetics of magnetoelastic domains without theoretical calculations yet. While beyond the scope of the current paper, such calculations using micromagnetic and microelastic simulations are highly desirable in future papers.

[1] A. E. Clark, K. B. Hathaway, M. Wun-Fogle, J. B. Restorff, T. A. Lograsso, V. M. Keppens, G. Petculescu, and R. A. Taylor, J. Appl. Phys. **93**, 8621 (2003).

[2] R. A. Kellogg, A. M. Russell, T. A. Lograsso, A. B. Flatau, A. E. Clark, and M. Wun-Fogle, Proceedings Smart Structures and Materials **5053**, 534 (2003).

[3] A. E. Clark, *Magnetostrictive Rare Earth*-Fe$_2$ *Compounds in Ferromagnetic Materials* (North-Holland, Amsterdam, 1980).

[4] B. Jaffe, W. R. Cook, and H. Jaffe, *Piezoelectric Ceramics* (Academic Press, London, 1971).

[5] T. Kakeshita and K. Ullakko, MRS Bull. **27**, 105 (2002).

[6] H. D. Chopra and M. Wuttig, Nature **521**, 340 (2015).

[7] H. D. Chopra, A. Ravishankar, M. S. Pacifico, and M. L. Forst, Phys. Status Solidi B **255**, 1800214 (2018).

[8] M. N. Tianen, D. J. Seguin, Y. U. Wang, and Y. M. Jin, Appl. Phys. Lett. **117**, 032401 (2020).

[9] S. Chikazumi and K. Suzuki, J. Phys. Soc. Jpn. **10**, 523 (1955).

[10] A. Hubert and R. Schäer, *Magnetic Domains: The Analysis of Magnetic Microstructures* (Springer, Berlin, 1998).

[11] C. Mudivarthi, S. M. Na, R. Schaefer, M. Laver, M. Wuttig, and A. B. Flatau, J. Magn. Magn. Mater. **322**, 2023 (2010).

[12] R. W. DeBlois and C. D. Graham, Jr., J. Appl. Phys. **29**, 931 (1958).

[13] R. Schäfer and S. Schinnerling, Phys. Rev. B **101**, 214430 (2020).

[14] L. Néel, Cah. Phys. **25**, 21 (1944).

[15] H. J. Williams, Phys. Rev. **71**, 646 (1947).

[16] M. N. Tianen and Y. M. Jin, J. Appl. Phys. **128**, 163904 (2020).

[17] V. W. Stephan, Exp. Tech. Phys. **4**, 153 (1956).

[18] V. W. Stephan, Exp. Tech. Phys. **5**, 145 (1957).

[19] G. Raghunath and A. B. Flatau, J. Appl. Phys. **117**, 17E704 (2015).

[20] S. Asano, S. Fujieda, S. Hashi, K. Ishiyama, T. Fukuda, and S. Suzuki, IEEE Magn. Lett. **8**, 6101004 (2017).

[21] Y. He, J. M. D. Coey, R. Schaefer, and C. Jiang, Phys. Rev. Materials **2**, 014412 (2018).